Optics Communications 291 (2013) 291–298

Contents lists available at SciVerse ScienceDirect

Optics Communications

journal homepage: www.elsevier.com/locate/optcom

Frequency noise performances of a Ti:sapphire optical frequency comb stabilized to an optical reference

D.V. Sutyrin [a,b], N. Poli [a], N. Beverini [b], S.V. Chepurov [c], M. Prevedelli [d], M. Schioppo [a], F. Sorrentino [a], M.G. Tarallo [a], G.M. Tino [a,*]

[a] Dipartimento di Fisica e Astronomia and LENS, Università di Firenze; Istituto Nazionale di Fisica Nucleare, Sezione di Firenze, Via Sansone, 1, 50019 Sesto Fiorentino, Italy
[b] Dipartimento di Fisica e CNISM, Università di Pisa, Largo Pontecorvo 3, Pisa, Italy
[c] Institute of Laser Physics SB RAS, Ac. Lavrentyev's prosp., 13/3, Novosibirsk 630090, Russia
[d] Dipartimento di Fisica, Università di Bologna, Via Irnerio 46, 40126 Bologna, Italy

ARTICLE INFO

Article history:
Received 4 August 2011
Received in revised form
30 October 2012
Accepted 14 November 2012
Available online 5 December 2012

Keywords:
Femtosecond laser
Optical frequency comb
Optical clock
Frequency noise
Strontium
Comb tooth linewidth

ABSTRACT

We report on a detailed analysis of frequency noise and intensity dynamics of a free-running femtosecond Ti:sapphire optical frequency comb (OFC) pumped by a multi-mode 532 nm laser. We have used these results for phase locking the OFC to a Hz-wide, cavity stabilized, 698 nm semiconductor laser. An analysis of the in-loop error signals and an estimation of Allan deviation indicates a lower limit for the frequency stability of the OFC at the level of $\sim 5.3 \times 10^{-14}$ for 125 ms integration time comparable with the clock laser frequency stability over the entire OFC spectrum. The noise transfer processes between the pump laser and the Ti:sapphire laser have been studied in detail, comparing the resulting frequency noise of the OFC output spectrum with both a single-mode and a multi-mode pump lasers. In the latter case, we employed a pump beam steering control to maintain an OFC regime with a minimum impact of pump laser amplitude noise on the carrier-envelope offset frequency.

1. Introduction

Optical frequency combs (OFCs) are nowadays used in many applications including optical frequency metrology [1], low-phase-noise microwave generation [2,3], calibration of astronomical spectra [4] and searches for variations of fundamental constants [5,6]. For all of these applications, in which high frequency stability is requested, a simultaneous control of the two degrees of freedom of the OFC, the laser carrier-envelope offset frequency (CEO) f_{CEO} and the repetition rate frequency f_{rep}, are demanded.

The noise properties and dynamics of OFCs are still under investigation, in order to further improve the frequency stability of the output spectrum. The quantum-limited noise properties of mode-locked lasers were first treated by Haus and Mecozzi based on soliton perturbation theory in [7]. More recent works extend the model of Haus and Mecozzi [8,9], including also technical noise contributions [10,11] and the effects of gain dynamics [12]. The noise properties due to the spontaneous emission were instead studied in the work of Wahlstrand et al. [13].

At the same time the fixed point formalism was introduced by Telle, Havercamp and coworkers in [14,15]. The formalism was used in several works to estimate the frequency noise of the optical spectrum of femtosecond fiber lasers [10,11,16]. Moreover, it has been shown that for each type of noise source there is an optimum pivot point for the control of the optical spectrum [17].

In this paper we focus on the study of frequency noise properties and dynamics of a self-referenced free-running Ti:sapphire OFC pumped by a multi-mode laser. In particular, we have characterized intensity-related dynamics of our Ti:sapphire laser by comparing the f_{CEO} frequency noise using different 532 nm laser pumps (a single mode Coherent Verdi V5 (sml) and a multi-mode Spectra Physics Millennia Xs (mml)). Due to the non-linear dependence of the f_{CEO} on intracavity power, we were able to choose an operating regime where the f_{CEO} is less sensitive to the pump laser amplitude noise, and to stabilize the f_{CEO} at mHz level with a mml pump. Moreover, we have determined the frequency stability of the OFC upper limit by testing it experimentally and lower limit from the calculations of the in-loop error signals.

The paper is organized as following. In Section 2 we describe setup components involving in the experiments. Section 3

* Corresponding author.
E-mail addresses: Denis.Sutyrin@fi.infn.it (D.V. Sutyrin), poli@lens.unifi.it (N. Poli), Guglielmo.Tino@fi.infn.it (G.M. Tino).

0030-4018/$ - see front matter © 2012 Elsevier B.V. All rights reserved.
http://dx.doi.org/10.1016/j.optcom.2012.11.045

introduces free-running OFC dynamics and frequency noise. We conclude this section with an estimation of free-running OFC teeth linewidth and their comparison with measurements. The results of this section we used to stabilize f_{CEO} with sml and mml, as we describe it in Section 4. Section 5 shows the results of the repetition rate frequency stabilization and an estimation of OFC frequency stability lower limit. In addition, in Section 6, we present a test of the impact of supercontinuum noise on OFC tooth linewidth. Finally, conclusions are presented in Section 7.

2. Experimental setup

A schematic view of the experimental setup is presented in Fig. 1. Our OFC is based on a home-built prismless femtosecond Ti:sapphire laser, with a pulse duration of 50 fs [22]. The self-mode-locked laser has a repetition rate of $\sim$294.5 MHz and an average output power of more than 700 mW (in mode-locked operation) with 4.5 W pump power coming from the mml or the sml. A detailed design description of the Ti:sapphire optical cavity has already been presented elsewhere [23]. The emission spectrum of the laser is centered around 810 nm with a typical FWHM of about 17 nm. The laser output is then coupled into a photonic crystal fiber (PCF) (Femtowhite 800), that broadens the spectrum to more than an octave (from $\sim$480 nm up to $\sim$1100 nm). The maximum power at the PCF output can reach 350 mW, but in order to reduce the wideband frequency noise generated in the fiber at high intensity, under typical working conditions the output power is reduced to less than 250 mW.

The optical frequency reference, used to stabilize the OFC, is a 698 nm semiconductor laser source employed in high resolution spectroscopy of the doubly forbidden $^1S_0-^3P_0$ clock transition in atomic strontium. A second semiconductor laser at 689 nm, resonant with the $^1S_0-^3P_1$ intercombination transition in atomic strontium, has also been employed to perform preliminary optical frequency comparisons with the stabilized OFC [18]. Further details about the experimental setup of both laser systems can be found respectively in [19,21]. Briefly, the first laser source is an extended cavity 698 nm diode laser (Littrow configuration) frequency stabilized with a two-steps Pound–Drever–Hall lock to high finesse optical cavities. The relative frequency stability of the 698 nm laser is $\sigma_y = 2\times10^{-15}$ for integration times between 1 s and 100 s [19]. The second source is a 689 nm extended cavity diode laser, frequency stabilized on a medium finesse cavity ($\sim10^4$) [20].

As shown in Fig. 1 the stabilized laser sources, the OFC and the strontium cold atom source are located in two separated laboratories, respectively at Dipartimento di Fisica ed Astronomia (UNIFI) and at European Laboratory for Non-Linear Spectroscopy (LENS). The light from the stabilized 689 nm laser is then transferred between the two labs through a 200 m fiber link [19]. After the propagation in the fiber without fiber noise compensation [19], the 689 nm laser shows a typical fast linewidth of the order of some kHz.

A radio-frequency (RF) 10 MHz reference to which we compared our stabilized OFC is a high-quality quartz oscillator slaved to the global positioning system (GPS) signal. The frequency stability of this reference is: $\sigma(1-4\ \mathrm{s}) = 6\times10^{-13}$, $\sigma(10\ \mathrm{s}) = 9\times10^{-13}$, $\sigma(100\ \mathrm{s}) = 2\times10^{-12}$, $\sigma(1000\ \mathrm{s}) = 2\times10^{-12}$. Then, at approximately 4000 s the servo loop on GPS signal steers the quartz giving a typical instability of $\sigma(4000-10000\ \mathrm{s}) = 2\times10^{-13}$.

The stabilization of the OFC f_{rep} is achieved using a 1/4 in. diameter flat folding mirror with zero dispersion that has been placed in the cavity to allow fast (up to 40 kHz) control of the cavity length through a piezoelectric transducer (PZT). A second PZT, placed on the output coupler, allows a slow control of the cavity length. In order to separate light at 698 nm from the output of the PCF we use a dichroic mirror and a 5 nm-wide passband filter centered at $\lambda = 695$ nm. After this filter we obtain about 1 mW of the OFC radiation at 698 nm. After a correction for the beam astigmatism by two cylindrical lenses, the OFC light is finally superimposed with the light from the 698 nm laser on a polarizing beam splitter and sent to a fast (300 MHz bandwidth) Si photodetector. To improve the S/N ratio of the f_{b698} beatnote an

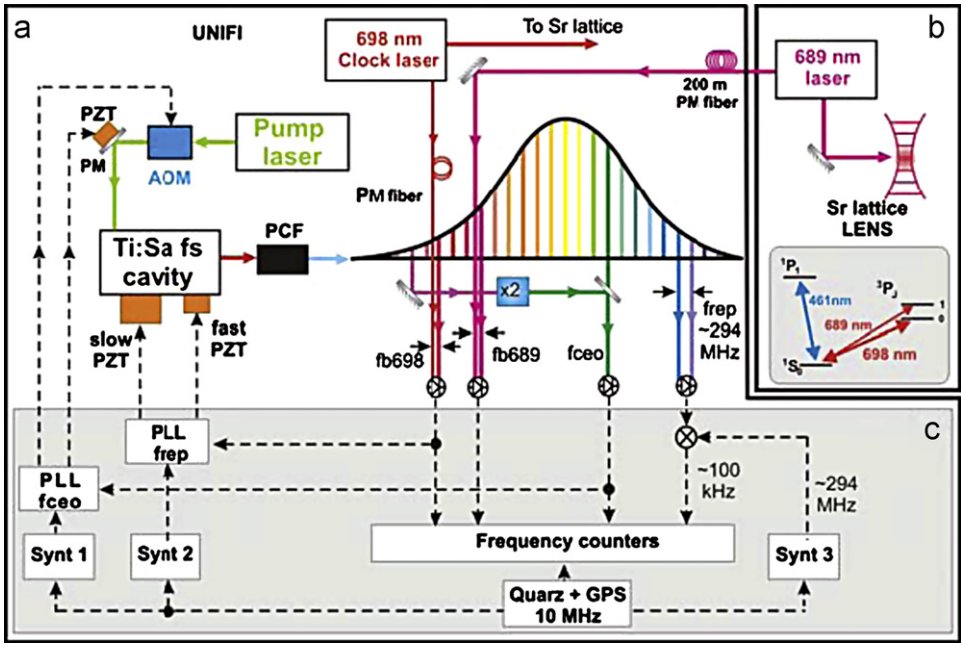

Fig. 1. Schematic view of the experimental apparatus with details of the optical path (a) and the electronics employed for stabilization of the OFC (c). Two frequency stabilized lasers respectively at 698 nm (resonant with strontium clock transition $^1S_0-^3P_0$) and 689 nm (b) (stabilized on the strontium second stage cooling transition $^1S_0-^3P_1$) are employed for the frequency stabilization of the OFC and for optical frequency ratio measurement. PM fiber, polarization-maintaining optical fiber; PCF, photonic crystal fiber; PLL, phase-locked loop; Synt, synthesizer; AOM, acousto-optical modulator; PM, pump mirror.

additional single cavity optical filter centered at 698 nm with a bandwidth of 0.3 nm is used. After this filter typical power levels are 2.70 mW from the clock laser and 180 μW from the femtosecond laser. In this condition, the f_{b698} signal is typically observed with a S/N ratio of 40 dB in 300 kHz bandwidth.

The f_{CEO} signal is measured by means of a standard f–2f interferometer [24] inserting in one arm of the interferometer a 3 mm-long BBO crystal for the second harmonic generation. The two beams at the output of the interferometer are sent to a fast Si photodetector. The typical S/N of the f_{CEO} signal, after a proper filtering and amplification, is about 40 dB in 300 kHz bandwidth.

In Fig. 1 the experimental apparatus used for the stabilization of f_{rep} and f_{CEO} is presented. The signals coming from photodetectors are amplified (typically 50 dB) and filtered with tunable RF cavity filters and finally sent to frequency counters and locking electronics. For phase-locking the beatnotes to reference RF signals, digital phase and frequency detectors (PFD) are employed. The reference RF signals are produced by a direct digital synthesizers, clocked by the 10 MHz reference signal. For the stabilization of f_{rep}, the f_{b698} signal is sent to the second input channel of the corresponding PFD. The error signal from the PFD is then processed by a proportional-integral-derivative (PID) amplifier, split in two channels and sent respectively to the "slow" and "fast" PZTs acting on the two cavity mirrors.

For f_{CEO} stabilization, similar electronics is employed. Here the slow frequency drifts are corrected through a PZT that changes the position of the pump mirror [25], while fast frequency fluctuations (up to 100 kHz) are corrected by changing the pump laser power with an acousto-optical modulator (AOM).

3. The free-running OFC intensity dynamics and frequency noise

To optimize the controls for f_{CEO} and f_{rep} we studied in detail the OFC intensity-related dynamics, determining the main frequency noise sources for the free-running OFC spectrum. Finally, the estimation of frequency noise of each OFC tooth has been compared with the experimental measurements of the f_{CEO} and f_{b698} signal linewidths.

3.1. Fixed point formalism

The power of the fixed-point formalism used to describe intracavity noise terms for a femtosecond fiber laser was demonstrated by Newbury and Swann [11]. We use the same approach to describe the frequency noise of our Ti:sapphire OFC. In the fixed point model each source of perturbation e.g. pump power, laser cavity, pump beam fluctuations, etc., will cause the comb to expand or to contract about a single fixed frequency, $\nu_0^X = n_0^X f_{rep} + f_{CEO}$, where $n_0^X = (\delta f_{CEO}/\delta X)/(\delta f_{rep}/\delta X)$, and X is the perturbation source [11,14,15]. The last equation implies that ν_0^X can be experimentally measured by changing a given parameter (e.g. pump power, cavity length, pump beam position) and by measuring the resulting change of f_{rep} and f_{CEO}. To measure the low-frequency response of the OFC to different parameter variations, we applied a weak, low frequency (1–10 Hz), periodic modulation to the pump power, to the laser cavity length and to the control voltage of the PZT attached to the pump mirror, and we recorded the resulting modulation of f_{CEO} and f_{rep} using frequency counters. These measurements were repeated for different values of the modulation frequency between 1 Hz and 10 Hz, thus generating a series of values of $\delta f_{CEO}/\delta X$ and $\delta f_{rep}/\delta X$, for each perturbation X. Even if for this frequency range we did not observe any dependence of these parameters on frequency, in general for fast perturbations the fixed point can depend strongly on frequency (see for example the full transfer function study by Schilt et al. [26]). However, we show here how a simple linear approximation already gives a good estimation of fixed points, allowing for a calculation of OFC frequency noise which results in good agreement with experimental data (see Fig. 4 at the end of this section).

3.2. Characterization of the frequency noise terms

To develop a quantitative picture of the OFC frequency noise, we will describe the frequency noise of each tooth of the comb through its noise power spectral density (PSD), $\int_0^\infty S_{vn} df = \sigma_n^2$, where $\sigma_n^2 = \langle \delta f^2 \rangle$ are the mean squared fluctuations of comb mode of index n. The total frequency noise PSD from multiple, uncorrelated noise sources is calculated by simply adding up the noise PSDs from the various sources, giving similarly as in [11]: $S_{vn}(f) = (S_{vn}^L(f) + S_{vn}^P(f) + S_{vn}^{ASE}(f)) + (S_{vn}^{SC}(f) + S_{vn}^{ShN}(f))$, where $S_{vn}^L(f)$ is the cavity length noise, $S_{vn}^P(f)$ is the amplitude noise of the pump laser and $S_{vn}^{ASE}(f)$ is the amplified spontaneous emission (ASE) PSDs. These intracavity noise terms can be described using the fixed-point formalism as [11]

$$S_{vn}^X(f) = (\nu_n - \nu_0^X)^2 s_{rep}^X(f), \tag{1}$$

where $s_{rep}^X(f) = f_{rep}^{-2}(\delta f_{rep}/\delta X)^2 s^X(f)$ is the PSD of the fractional repetition-rate fluctuations driven by the fluctuations in the parameter X.

Other extracavity noise terms are respectively given by the supercontinuum noise PSD $S_{vn}^{SC}(f)$ and the shot noise PSD $S_{vn}^{ShN}(f)$.

3.3. OFC intensity-related dynamics

As pointed out in [27], in Ti:sapphire OFCs, for which the femtosecond pulse spectrum does not fill up the whole available optical spectrum bandwidth, f_{CEO} shows a non-linear dependence as a function of pump laser intensity. Fig. 2 demonstrates a typical dependence of f_{CEO} as a function of the pump power for our femtosecond laser. In particular we can observe a stationary point of f_{CEO} at about 4.5 ± 0.2 W (often referred as "turning point" [27]). For this value of pump power f_{CEO} is insensitive to intensity changes in the cavity. On the other hand, the f_{CEO} sensitivity to intensity change can vary in function of cavity alignment. Near to the working point the linewidth of the f_{CEO} signal becomes smaller reaching its minimum of $\Delta\nu = 15$ kHz at 4.36 W, as shown in Fig. 2. This value is also related to the rather high intracavity

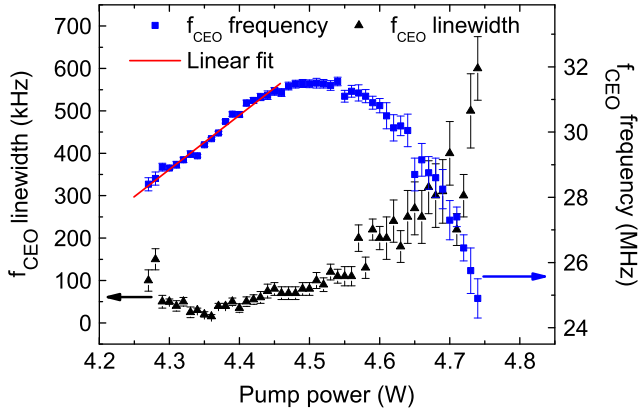

Fig. 2. Center frequency (squares) and linewidth (triangles) of the f_{CEO} signal detected after f–2f interferometer, as a function of pump power. For this measurement the mml pump has been employed. The measured linewidth reaches a minimum of 15 kHz at pump power P=4.35 W near to the turning point for f_{CEO} (see text for details).

dispersion of our OFC ($\sim -400\ \mathrm{fs}^2$) and might be decreased by designing a cavity with smaller dispersion (see also Section 6).

Even if f_{CEO} has in general a non-linear behavior in function of other fluctuations, it is still possible to determine all the fixed points in regions where f_{CEO} has a linear dependence far from the turning points (see Fig. 2).

In this case, the measured values of fixed frequencies are $\nu_0^P = 147$ THz and $\nu_0^L = 2.5$ THz, while the OFC spectrum spans from 272.7 THz to 625 THz.

3.4. Intracavity and extracavity noise sources

The main contribution to the linewidth of each OFC tooth comes from the intracavity noise terms. The dominating intracavity terms are: $S_{vn}^P(f)$, $S_{vn}^L(f)$.

A pump laser can introduce noise through its beam-pointing instability and its amplitude noise. The cavity length instead can fluctuate due to many environmental effects: temperature changes, sub-acoustic and acoustic vibrations from the optical table supports and temperature induced fluctuations of the index of refraction of air.

3.5. Cavity length perturbations

We estimated upper and lower limits of the cavity length fluctuation term $S_{vn}^L(f)$ from the measured passive stability of the free-running f_{rep}. A lower and an upper limits of $|\sigma_{rep}|$ are 0.25 and 0.50 Hz respectively.

Supposing that f_{rep} fluctuations are caused only by cavity length fluctuations (with a negligibly small contribution due to other effects) we can extract a value for the lower and upper limits of the cavity length fluctuations $\langle|\delta L^{meas}|\rangle \approx 433-865$ pm (calculated for the actual cavity length of ~ 0.5 m). From this, we then estimate the value of the PSD fractional frequency fluctuation induced by the cavity length fluctuations as follows:

$$s_{rep}^L(1\ \mathrm{Hz}) = B \times s^L(1\ \mathrm{Hz}) = 7.22 \times 10^{-19} - 2.89 \times 10^{-18}, \quad (2)$$

where $s^L(1\ \mathrm{Hz}) = (\delta L/L)^2 = [(c\delta f_{rep}/2f_{rep}^2) \times (2f_{rep}/c)]^2$ and the sensitivity parameter is $B = \left[(L\delta f_{rep})/(f_{rep}\delta L)\right]^2 = 1$.

In fact, the $1/f$ frequency dependence of s^L (in the range 1 Hz–1 MHz) here represents an overestimation of the real cavity length noise, induced mainly by mechanical fluctuations. Here, for simplicity of the model, noise filtering effect due to the presence of mechanical resonances of the cavity have been neglected. However, as will be demonstrated later in this paragraph, this simple estimation gives correct results in terms of estimated comb teeth linewidth.

3.6. Amplitude noise from pump lasers

As mentioned in the previous section, two different types of commercial pump lasers have been tested with our OFC: sml and mml. As shown in Fig. 3 in the low frequency range (up to 7 kHz) the measured amplitude noise for the sml is typically higher than that of the mml. On the other hand, in the high frequency range starting from 10 kHz, the mml presents a higher noise (similar spectra have also been observed in [12,28]).

Fitting the data, we find for sml a relative intensity noise (RIN) of $s^{RINsml} = 5 \times 10^{-5}/f\ \mathrm{Hz}^{-1}$ PSD, while for mml $s^{RINmml} = 3 \times 10^{-8}/f^2\ \mathrm{Hz}^{-1}$ (upper limit) and $s^{RINmml} = 1 \times 10^{-8}/f^2\ \mathrm{Hz}^{-1}$. The PSD describing the fractional frequency fluctuation in terms of the pump laser RIN can then be calculated as [11]

$$s_{rep}^P(f) = Cs^{RIN}, \quad (3)$$

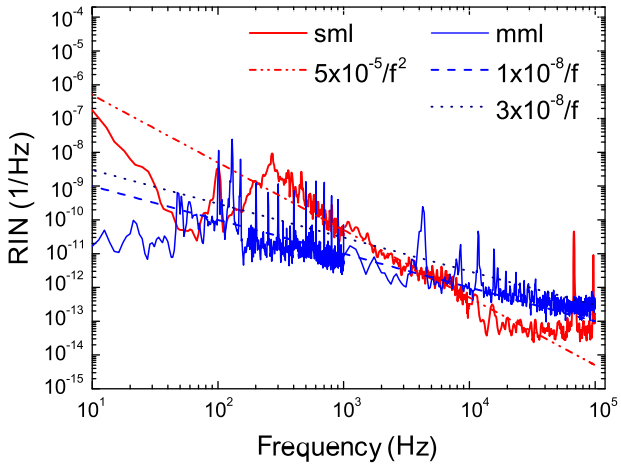

Fig. 3. Measured RIN spectral densities of sml (red) and mml (blue) and their fits for frequency noise PSD calculations. (For interpretation of the references to color in this figure legend, the reader is referred to the web version of this article.)

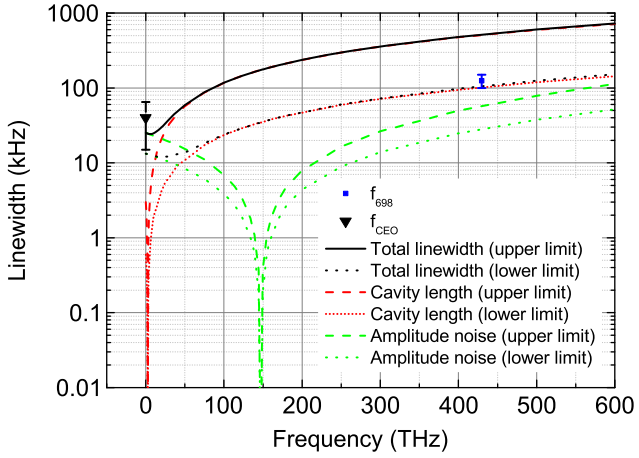

Fig. 4. The calculated OFC tooth linewidth across the free-running OFC spectrum for pump laser amplitude noise for mml pump case with a fixed point at ~147 THz (green dots for the lower case, green dash for the upper case) and the cavity length fluctuations (red dots for the lower case, red dash for the upper case) with the measured f_{698} (blue square) and f_{CEO} (black triangle) linewidths. The f_{CEO} linewidth is measured near to the turning point. The total OFC tooth linewidth is shown by the black solid curve (upper limit) and by the black dots (lower limit). (For interpretation of the references to color in this figure legend, the reader is referred to the web version of this article.)

where the repetition rate sensitivity parameter, estimated for the typical power level for our OFC, is $C = [(P\delta f_{rep})/(\delta P f_{rep})]^2 = 1.3 \times 10^{-12}$. By using Eq. (3) we calculated the two values $s_{rep}^{mml}(1\ \mathrm{Hz}) = 13 \times 10^{-21}\ \mathrm{Hz}^{-1}$ and $s_{rep}^{mml}(1\ \mathrm{Hz}) = 39 \times 10^{-21}\ \mathrm{Hz}^{-1}$ for the lower and the upper limit of mml amplitude noise respectively and the single value for the sml $s_{rep}^{sml}(1\ \mathrm{Hz}) = 6.5 \times 10^{-17}\ \mathrm{Hz}^{-1}$.

3.7. ASE-induced noise terms

The ASE-induced noise leads to fluctuations of different cavity parameters that have also different fixed points. However, as was discussed in [11], it can be described by two effects: a timing jitter and a phase jitter. The timing jitter contribution dominates for comb teeth that are far away from the timing jitter fixed point (typically located near to the OFC carrier frequency) $\nu_0^{ASE,t} \simeq \nu_c$ [11]. Using the equation for the timing jitter from [11] we get a value of $s_{rep}^{ASE,t}(1\ \mathrm{Hz}) = 5.6 \times 10^{-28}\ \mathrm{Hz}^{-1}$, that is negligible.

The phase jitter is instead due to the Schawlow–Townes limit [8,9,29], which is the same for all modes. In our case this term is

equal to $\sim 10^{-4}$ Hz^2/Hz and then it is also negligible compared to other technical noise terms.

3.8. Shot noise and supercontinuum generation

The extra-cavity noise is given mainly by shot noise and supercontinuum noise. Shot noise results in white phase noise, limiting the signal-to-noise ratio (SNR) as $\mathrm{SNR} = \sqrt{N_n}$, where N_n is the number of photons associated with the nth mode. For typical detected power of 50 nJ per OFC tooth, the calculated SNR is equal to ≈ 50 dB. However, the power per tooth clearly varies strongly with wavelength. Moreover, this represents a lower limit to the phase-noise floor, which will likely be limited in practice by the noise generated during the supercontinuum formation, as discussed below.

As was established experimentally for Ti:sapphire OFC, the supercontinuum generation process generates a consistent excess of amplitude and phase noise [34–39].

In our case, the impact of supercontinuum generation process on OFC tooth linewidth is supposed to be smaller compared to other effects as the cavity length and the pump laser amplitude fluctuations in the frequency range between 1 Hz and 1 MHz. This assumption has been also verified with an experimental test described below in Section 6. In conclusion, all the estimated noise contributions are summarized in Table 1.

3.9. OFC tooth linewidth estimation for free-running operation

From the calculated frequency noise PSD we can estimate the linewidth of an OFC tooth using an analytical expression for the root mean square (rms) linewidth: $\Delta\nu_{rms} = \int_0^\infty S_{\nu n}(f)\, df$.

Fig. 4 shows the calculated linewidth as a function of OFC tooth frequency specifically in the case of mml pump. As expected, the main contribution to OFC tooth frequency noise comes from cavity length fluctuations.

The big gap between upper and lower limit in the estimation of the tooth linewidth due to cavity length fluctuations (~ 414 kHz at around 434 THz) is related to different working conditions that we observed in our cavity. Indeed, the working point of the free-running comb can change even within the same day due to environmental conditions changes (mostly due to the room temperature variations).

Anyhow, we compared the results of these estimations with experimental measurements of comb teeth linewidth. In particular, the measured beatnote signal between the OFC and the clock laser (at around 434 THz) has a linewidth of 125 ± 25 kHz, in agreement with the lower limit predicted by the model.

In Fig. 4 is also shown a comparison of the measured f_{CEO} linewidth (measured near to the turning point) with respect to the estimated theoretical linewidth. Again, we obtained a good agreement with the model.

4. f_{CEO} stabilization; comparison between sml and mml pumps

The best results on OFC frequency stabilization have been obtained by acting independently on the two degrees of freedom of the comb, or through diagonalization of the comb control on f_{rep} and f_{CEO}. In terms of the fixed point model, a control parameter of the OFC to which corresponds a fixed point frequency $\nu_0^X \sim f_{CEO}$ is adequate to stabilize the f_{rep}, while a control with $\nu_0^X \sim \nu_c$ can be used to stabilize f_{CEO}. For example, even if pump power modulation is typically used to control f_{CEO}, its efficiency depends strongly on the fixed point value. Indeed, when the fixed point lies near to the center of the optical spectrum of the OFC, the pump power modulation become a more adequate control for the stabilization of f_{rep}, as also recommended by Walker et al. in [30] and used in [31].

In our case, considering the fixed point values for the free-running OFC, it follows that the cavity length fluctuations δL will affect mostly f_{rep}, while keeping f_{CEO} almost unchanged. Therefore, the appropriate way to control the comb teeth distance is, as usual, to change the cavity length. On the other hand, both pump power modulation and pump beam position have instead an impact on both f_{rep} and on f_{CEO} and in our case they have been chosen to control f_{CEO}.

The pump power modulation is often performed by an AOM interposed between the pump and the Ti:sapphire cavity. However, the finite response time of the pump gain and the AOM introduce a phase delay into the closed-loop transfer function that limits the loop bandwidth (see the OFC feedback loop analysis in [12]). This bandwidth limit represents a problem with the mml pump, because it has a higher amplitude noise at higher frequencies when compared with a sml, which typically cannot be effectively compensated (see Fig. 3 and results in [12,28]). In our case, the sml pump has a strong resonance around 100 kHz, which is not typical and this explains the big difference between the integrated phase noise under closed loop condition (Fig. 5) obtained with mml and sml pumps.

A way to overcome an AOM limitation to reduce the effect of mml amplitude noise on f_{CEO} is to operate the OFC near the turning point. While the reduction of sensitivity can be very large, in the case of mml and high intracavity dispersion, the region near turning point, can be very small.

In order to have an additional long term control on the operating regime of the cavity, maintaining it near to the turning point, we

Table 1
Fixed point, frequency dependence, and magnitude of the various contributions to the frequency noise on the OFC lines.

Noise term	Fixed point	Frequency dependence	$s_{rep}^X(1)[\mathrm{Hz}^{-1}]$
Environmental (length)	~ 2.5 THz	f^{-1}	Lower $\sim 7.22 \times 10^{-19}$, Upper $\sim 2.89 \times 10^{-18}$;
Pump noise	~ 147 THz	f^{-1} – mml	Lower13.0×10^{-21}, Upper 39.0×10^{-21};
		f^{-2} – sml for 10 Hz–100 kHz; f^0 for >100 kHz	1.3×10^{-17};
Schawlow–Townes limit	NA	f^0	$\sim 5.4 \times 10^{-34}$
Intracavity ASE (quantum limit)	~ 375 THz	f^0	5.6×10^{-28}
Pump beam shift	~ 117 THz	–	–
Supercontinuum and shot noise	NA	f^2	–

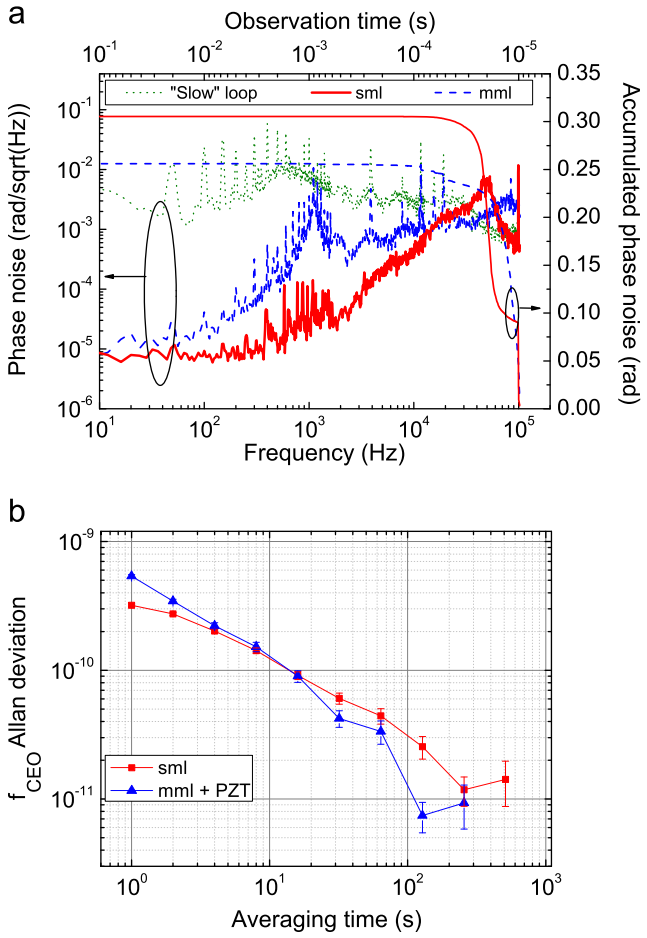

Fig. 5. The noise spectral densities and the corresponding Allan deviations of the phase-locked f_{CEO} (a) and (b). (a) The measured phase noise of the locked f_{CEO}. Upper green dot curve: slow loop f_{CEO} phase noise (mml case) measured with a slow servo loop (<1 kHz) acting on the pump laser AOM, when f_{CEO} was weakly locked at low frequencies, middle blue dash curve and lower red solid curves: the closed loop f_{CEO} phase noise with mml and sml pumps respectively. Blue dash and red solid curves show the accumulated phase noise respectively for mml and sml. Ellipses and arrows indicates to which vertical scale the curves are referred. (b) The Allan deviation for the f_{CEO} estimated from the frequency counting measurement, red squares and blue triangles are for the sml and mml cases respectively. (For interpretation of the references to color in this figure legend, the reader is referred to the web version of this article.)

implemented an additional control to shift the pump beam [25]. In fact, we choose to work in an operating regime not far from the turning point, where the f_{CEO}/P relation is linear (area of linear fit in Fig. 2), and where the linewidth of the f_{CEO} signal is minimum (see Fig. 2).

Even if this control affects both f_{rep} and f_{CEO} (because of the corresponding fixed point frequency ~ 117 THz), this flaw is however not important, because we use this mechanism only as a second slow loop, while the fast corrections are always given by the pump power control. The error signal which drives the AOM is further integrated and sent to the pump beam PZT, controlling the pump beam displacement (in the horizontal plane) with respect to the femtosecond cavity. In our experimental conditions the maximum displacement is about 8.5 μm corresponding to a maximum f_{CEO} shift of 15 MHz. In this way we perform the CEO phase stabilization by employing a double feedback loop [32].

The results for the f_{CEO} stabilization with different pump lasers are presented in Fig. 5. The phase noise spectra differ both in the high and low frequency regimes, the accumulated phase noise are $\Delta\varphi_{CEO}^{mml}=0.256$ rad and $\Delta\varphi_{CEO}^{sml}=0.305$ rad respectively. This result is mainly given by the use of the pump beam steering control for long term f_{CEO} stabilization in the case of mml and by the resonance at around 100 kHz in sml. The result of the pump beam shift control can be seen in Fig. 5, where the phase noise of f_{CEO} at low-frequencies in the case of mml is close to the phase noise of f_{CEO} in the case of sml. In turn, the f_{CEO} phase noise in the case of sml at low frequencies is limited by the phase noise of our PFD at the level of 8×10^{-6} rad/$\sqrt{\text{Hz}}$. The f_{CEO} phase noise at Fourier frequencies of 10–50 Hz is found to be lower by 1.5–7 times comparing with the results in [12]. While for the sml pump it is possible to reduce the phase noise at low Fourier frequencies, it is hard to compensate the contribution introduced by the resonance at around 100 kHz (see Fig. 3). The large phase shift introduced by this resonance limits the PLL servo bandwidth down to about 40 kHz with sml pump, while it can be extended to 120 kHz in the case of mml pump. A drawback in the use of Millennia Xs mml pump in our experimental setup is the presence of uncompensated higher acoustic and sub-acoustic noise produced by the laser head which is directly coupled into the Ti:sapphire cavity. The impact of the pump laser amplitude noise is increased by the high intracavity dispersion of our OFC.

5. Repetition rate stabilization and comparison with 689 nm optical reference

The phase noise of the f_{rep} stabilized on the clock laser at 698 nm, measured against our RF reference, is shown in Fig. 6a. The loop bandwidth is ~ 40 kHz. Fig. 6b shows the Allan deviation of f_{rep}, with a minimum deviation of about 150 μHz at 100 s.

We tested also the stability of the locked frequency comb directly in the optical region, by measuring the optical frequency ratio between the clock laser and a stabilized 689 nm laser. For this measurement, we counted the beatnote of the OFC with the 689 nm laser f_{b689} (transferred over the 200 m-long fiber link between the two laboratories) simultaneously with f_{CEO} and f_{rep}. The linewidth of the observed f_{b689} signal was about 2.5 kHz (see Fig. 7a), limited both by the residual frequency noise of the 689 nm laser and by the additional phase noise of the 200 m fiber link. This value sets an upper limit to the relative frequency stability of the optical frequency ratio at about 1×10^{-12} at 1 s (see Fig. 7b). The short term frequency stability measured by direct optical comparison is about a factor of three better with respect to the frequency stability obtained in absolute frequency measurements of our clock laser against our RF standard (optical-RF comparison).

5.1. Estimation of Allan deviation for different teeth of the stabilized OFC

To measure the frequency stability of a frequency comb one might perform tests at different wavelengths by employing several different stabilized laser sources. Since this represents an experimental challenge due to the limited availability of high stability laser sources in a wide frequency range, here we use a different method based on the analysis of in-loop servo signals used for the stabilization and of the beatnote signals with the optical reference.

In particular, the estimation is based on in-loop measurements of the frequency noise of f_{rep} and f_{CEO} under locking condition. When n_{ref}-th comb tooth at frequency ν_{nref} is locked to an optical reference ν_{ref}, the nth comb mode frequency noise is given by :

$$S_{\nu_n}=\left(\frac{n}{n_{ref}}\right)^2 S_{\nu nref}+\left(1-\frac{n}{n_{ref}}\right)^2 S_{CEO}. \tag{4}$$

Here we have neglected the cross-correlation term χ between the f_{CEO} noise and f_{rep} noise, since in our conditions all fixed points lie in a frequency range between f_{CEO} and ν_{nref} [11]. In this case it is possible to show that the cross-correlation term is always

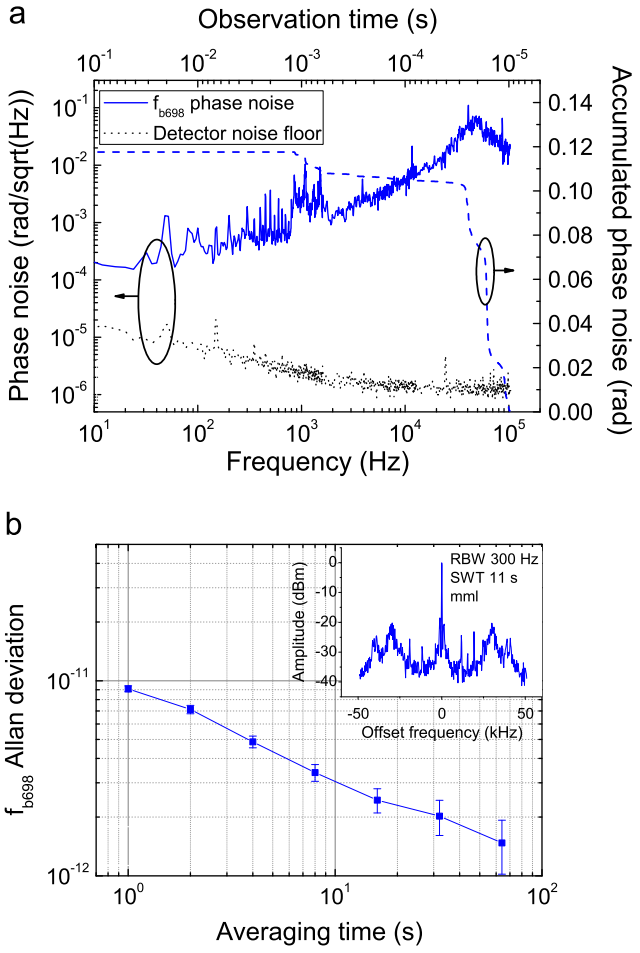

Fig. 6. The noise spectral densities and the corresponding Allan deviations of the phase-locked f_{b698} (a) and (b). (a) The measured phase noise of the stabilized f_{b698} (blue solid), phase and frequency detector noise floor (black dots). Blue dashes show the accumulated phase noise of the stabilized f_{b698}. (a) An in-loop signal. Ellipses and arrows indicates to which vertical scale the curves are referred. (b) The Allan deviation for the f_{b698} estimated from the frequency counting measurement (the recorded beatnote spectrum is shown in the inset). (For interpretation of the references to color in this figure legend, the reader is referred to the web version of this article.)

negative, thereby a reasonable upper limit to the residual frequency noise on the OFC teeth can be estimated by setting the cross-correlation to zero ($\chi = 0$) leading to Eq. (4). Since the optical reference centered at 698 nm is used to stabilize the OFC, and considering the OFC output spectrum (500 nm–1100 nm), the ratio n/n_{ref} lies between 0.63 and 1.45.

The Allan variance may be determined from the frequency noise spectrum $S_{\nu_n}(f)$ by the integral [33]

$$\sigma^2(\tau) = 2\int_0^\infty S_{\nu_n}(f)\frac{\sin^4(\pi f\tau)}{(\pi f\tau)^2}\,df. \tag{5}$$

Using the frequency noise measurements of the locked f_{CEO} and f_{b698} in-loop signals from Figs. 5 and 6a and Eq. (4), we calculated the Allan deviation at different integration times across the OFC. From the calculations, the relative frequency stability of the different OFC teeth was found to be constant across the OFC output spectrum with the value $\sim 5.3(5)\times 10^{-14}$ for 125 ms integration time. This value is consistent with the clock frequency stability measured at 130 ms integration time $\sigma_y = 1.15(1)\times 10^{-14}$ [19] it represents a lower limit for the frequency stability of OFC.

6. Experimental test of supercontinuum excess noise

To check the impact of supercontinuum noise on OFC tooth linewidth and *S*/*N* ratio in Section 3.8, we tested the OFC in a different regime. In particular, we changed the dispersion of the femtosecond Ti:sapphire laser from $-400\ \mathrm{fs}^2$ to $-175\ \mathrm{fs}^2$ by replacing the GTI mirror with one pair of chirped mirrors. With this configuration as shown in Fig. 8, the optical spectrum at the output of the cavity becomes much broader, spanning from 680 nm up to 880 nm with an output power of about 550 mW. In particular, the typical optical power of the OFC after two pass-band optical filters centered at 698 nm (5 nm and 0.3 nm wide) is about 500 μW. In this case, f_{b698} can be measured directly by beating the spectrum at the output of the cavity with clock laser light, bypassing the microstructure fiber.

Also in this case, the measured linewidth of the beatnote signal is of the order of 100 ± 20 kHz (RWB 30 kHz, SWT 67 ms) consistent with the previous determination (see Fig. 4) confirm-

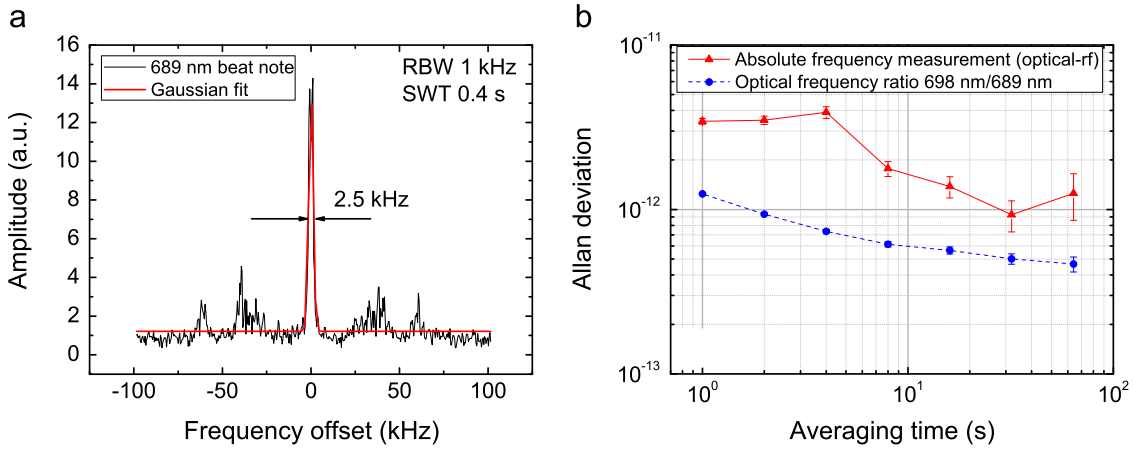

Fig. 7. Experimental results of the OFC stabilization to the clock laser at 698 nm. (a) Observed f_{689} signal after the propagation in a 200 m-long fiber (without fiber noise compensation). (b) Allan deviation for different experimental frequency data sets: absolute frequency measurements of 689 nm laser (red triangles), optical frequency ratio between 689 nm and 698 nm laser (blue circles). The Allan deviation estimated for the optical frequency ratio measurement is clearly limited by the 689 nm laser linewidth after propagation in the 200 m-long fiber and not by the comb stabilization. (For interpretation of the references to color in this figure legend, the reader is referred to the web version of this article.)

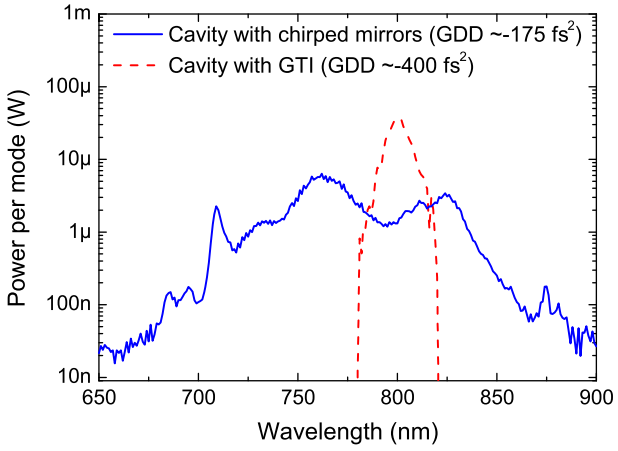

Fig. 8. Optical spectra of the Ti:sapphire cavity (without broadening in the PCF) for two different values of the intracavity dispersion: red dashed curve for GDD $\sim -400\ fs^2$, blue solid curve for GDD $\sim -175\ fs^2$. (For interpretation of the references to color in this figure legend, the reader is referred to the web version of this article.)

ing our initial hypothesis on extracavity noise terms (see Section 3.8). While the main contributions to the beatnote linewidth remain pump power amplitude fluctuations and cavity length fluctuations, in our case supercontinuum OFC noise gives a negligible contribution to the beatnote linewidth.

7. Conclusion

In this work we studied the frequency noise of a free-running home-build Ti:sapphire OFC pumped by mml. We estimated the free-running linewidth of each OFC tooth and compared two of them (at 698 nm and in the f_{CEO} frequency region) with measurements in good agreement with our model.

From the frequency noise analysis, we were able to optimize f_{CEO} stabilization loop implementing a pump beam steering control and using different kinds of pump lasers. We have demonstrated that the f_{CEO} can reach similar frequency stability either with sml or by using mml pumps. While this manuscript was under review, an independent study of Vernaleken et al. [40] confirmed this result.

We have phase-locked the OFC pumped by mml and sml to a laser with high spectral purity, operating at 698 nm, close to the frequency of the clock transition $^1S_0-^3P_0$ in neutral strontium atoms. We also performed out-of-loop first tests of the OFC stability by comparing it with a high quality quartz oscillator and with a second stabilized laser at 689 nm. As expected, the stabilized OFC demonstrated a better short term stability than absolute frequency measurements of optical frequencies against an RF reference.

A lower limit for the OFC frequency stability has been estimated from in-loop servo signals used for the OFC stabilization. The result of this analysis shows a stability of $\sim 5.3(5)\times 10^{-14}$ for 125 ms integration time, comparable to the frequency stability of our 698 nm clock laser.

Acknowledgments

We thank A. De Michele, B. Nyushkov, E. Maccioni and T. Mazzoni for their contribution in the early stage of the experiment, T.M. Fortier and A.A. Lugovoy for the careful reading of the manuscript. We also thank R. Ballerini, M. De Pas, M. Giuntini, A. Hajeb, A. Montori for technical assistance. This work is supported by LENS (under contract RII3 CT 2003 506350), ESA (under contract MAP C20579(SOC 2008)) and MIUR (under contract PRIN 2009 - prot. 2009ZJJBLX).

References

[1] Th. Udem, R. Holzwarth, T.W. Hänsch, Nature 416 (6877) (2002) 233.
[2] A. Bartels, S.A. Diddams, C.W. Oates, G. Wilpers, J.C. Bergquist, W.H. Oskay, L. Hollberg, Optics Letters 30 (6) (2005) 667.
[3] S.A. Diddams, M. Kirchner, T. Fortier, D. Braje, A.M. Weiner, L. Hollberg, Optics Express 17 (5) (2009) 3331.
[4] T. Steinmetz, T. Wilken, C. Araujo-Hauck, R. Holzwarth, T.W. Hansch, L. Pasquini, A. Manescau, S. D'Odorico, M.T. Murphy, T. Kentischer, W. Schmidt, Th. Udem, Science 321 (5894) (2008) 1335.
[5] S.G. Karshenboim, Canadian Journal of Physics 78 (7) (2000) 639.
[6] V.A. Dzuba, V.V. Flambaum, J.K. Webb, Physical Review A 59 (1) (1999) 230.
[7] H. Haus, A. Mecozzi, IEEE Journal of Quantum Electronics 29 (1993) 983.
[8] R. Paschotta, Applied Physics B 79 (2004) 153.
[9] R. Paschotta, Applied Physics B 79 (2004) 163.
[10] N. Newbury, B. Washburn, IEEE Journal of Quantum Electronics 41 (2005) 1388.
[11] N.R. Newbury, W.C. Swann, Journal of the Optical Society of America B 24 (2007) 1756.
[12] L. Matos, O.D. Mücke, J. Chen, F.X. Kärtner, Optics Express 14 (6) (2006) 2497.
[13] J.K. Wahlstrand, J.T. Willits, C.R. Menyuk, S.T. Cundiff, Optics Express 16 (23) (2008) 18624.
[14] H.R. Telle, B. Lipphardt, J. Stenger, Applied Physics B 74 (2002) 1.
[15] N. Haverkamp, H. Hundertmark, C. Fallnich, H.R. Telle, Applied Physics B 78 (2004) 321.
[16] B.R. Washburn, W.C. Swann, N. R Newbury, Optics Express 13 (2005) 10622.
[17] R. Paschotta, A. Schlatter, S.C. Zeller, H.R. Telle, U. Keller, Applied Physics B 82 (2006) 265.
[18] N. Poli, M.G. Tarallo, M. Schioppo, C.W. Oates, G.M. Tino, Applied Physics B 97 (2009) 27.
[19] M.G. Tarallo, N. Poli, M. Schioppo, D. Sutyrin, G.M. Tino, Applied Physics B 103 (2011) 17.
[20] G. Ferrari, P. Cancio, R. Drullinger, G. Giusfredi, N. Poli, M. Prevedelli, C. Toninelli, G.M. Tino, Physical Review Letters 91 (2003) 243002.
[21] N. Poli, G. Ferrari, M. Prevedelli, F. Sorrentino, R.E. Drullinger, G.M. Tino, Spectrochimica Acta A 63 (5) (2006) 981.
[22] N. Poli, M.G. Tarallo, M. Schioppo, C.W. Oates, S. Chepurov, D. Sutyrin, A. De Michele, N. Beverini, G.M. Tino, in: Proceedings of the Fifth International Symposium Modern Problems of Laser Physics (MPLP'2008) Novosibirsk, Russia, 24–30 August 2008, p. 327.
[23] N. Beverini, N. Poli, D. Sutyrin, F.-Y. Wang, M. Schioppo, M.G. Tarallo, G.M. Tino, in: SPIE proceedings ICONO 2010 Conference, 23–26 August 2010, Kazan, Russia.
[24] H.R. Telle, G. Steinmeyer, E.A. Dunlop, J. Stenger, D.H. Sutter, U. Keller, Applied Physics B 69 (1999) 327.
[25] W.-Y. Cheng, T.-H. Wu, S.-W. Huang, S.-Y. Lin, C.-M. Wu, Applied Physics B 92 (2008) 13, http://dx.doi.org/10.1007/s00340-008-3058-7.
[26] S. Schilt, V. Dolgovskiy, N. Bucalovic, L. Tombez, M. Stumpf, G. Di Domenico, C. Schori, S. Pekarek, A.E.H. Oehler, T. Südmeyer, U. Keller, U.P. Thomann, CLEO: 2011—Laser Applications to Photonic Applications CFK3, 2011.
[27] K.W. Holman, R.J. Jones, A. Marian, S.T. Cundiff, J. Ye, IEEE Journal of Selected Topics in Quantum Electronics 9 (4) (2003) 1018.
[28] S. Witte, R.T. Zinkstok, W. Hogervorst, K.S.E. Eikema, Applied Physics B 78 (1) (2004) 5.
[29] A.L. Schawlow, C.H. Townes, Physical Review 112 (1958) 1940.
[30] D.R. Walker, Th. Udem, Ch. Gohle, B. Stein, T.W. Hänsch, Applied Physics B 89 (2007) 535.
[31] D.C. Heinecke, A. Bartels, T.M. Fortier, D.A. Braje, L. Hollberg, S.A. Diddams, Physical Review A 80 (5) (2009) 053806.
[32] T.J. Yu, K.-H. Hong, H.-G. Choi, J.H. Sung, IlW. Choi, D.-K. Ko, J. Lee, J. Kim, D.E. Kim, Ch.H. Nam, Optics Express 15 (13) (2007) 8203.
[33] J. Rutman, F.L. Walls, Proceedings of IEEE 79 (1991) 952.
[34] N.R. Newbury, B.R. Washburn, K.L. Corwin, R.S. Windeler, Optics Letters 28 (11) (2003) 944.
[35] K.L. Corwin, N.R. Newbury, J.M. Dudley, S. Coen, S.A. Diddams, B.R. Washburn, K. Weber, R.S. Windeler, Applied Physics 77 (2003) 269.
[36] K.L. Corwin, N.R. Newbury, J.M. Dudley, S. Coen, S.A. Diddams, K. Weber, R.S. Windeler, Physical Review Letters 90 (11) (2003) 113904-1–113904-4.
[37] J.H. Ames, S. Gnosh, R.S. Windeler, A.L. Gaeta, S.T. Cundiff, Applied Physics 77 (2003) 279.
[38] BR. Washburn, N.R. Newbury, Optics Express 12 (10) (2004) 2166.
[39] T.M. Fortier, J. Ye, S.T. Cundiff, R.S. Windeler, Optics Letters 27 (6) (2002) 445.
[40] A. Vernaleken, B. Schmidt, M. Wolferstetter, T. Hänsch, R. Holzwarth, P. Hommelhoff, Optics Express 20 (16) (2012) 18387.